CHEMISTRY
AN ASIAN JOURNAL
www.chemasianj.org

Accepted Article

Title: Macrocycles All Aflutter: Substitution at an Allylic Center Reveals Conformational Dynamics of [13]-Macrodilactones

Authors: Kelli M Rutledge, Trevor Hamlin, Donna Baldisseri, Matthias Bickelhaupt, and Mark Wayne Peczuh

To be cited as: *Chem. Asian J.* 10.1002/asia.201700997

Link to VoR: http://dx.doi.org/10.1002/asia.201700997

A Journal of

ACES
Asian Chemical Editorial Society

A sister journal of Angewandte Chemie and Chemistry – A European Journal

WILEY-VCH

10.1002/asia.201700997

Macrocycles All Aflutter: Substitution at an Allylic Center Reveals Conformational Dynamics of [13]-Macrodilactones

Kelli M. Rutledge,[a] Trevor A. Hamlin,[b] Donna M. Baldisseri,[c] F. Matthias Bickelhaupt,[b],[d]* and Mark W. Peczuh[a]*

[a] Department of Chemistry, University of Connecticut, 55 N. Eagleville Road U-3060, Storrs, CT 06269, USA.
E-mail: mark.peczuh@uconn.edu

[b] Department of Theoretical Chemistry and Amsterdam Center for Multiscale Modeling, Vrije Universiteit Amsterdam, NL-1081 HV Amsterdam, The Netherlands.
E-mail: f.m.bickelhaupt@vu.nl

[c] Bruker BioSpin Corporation, 15 Fortune Drive, Manning Park, Billerica, MA 01821, USA.

[d] Institute of Molecules and Materials, Radboud University, 6525 AJ Nijmegen, The Netherlands.

10.1002/asia.201700997

TOC Graphic/Graphic Abstract

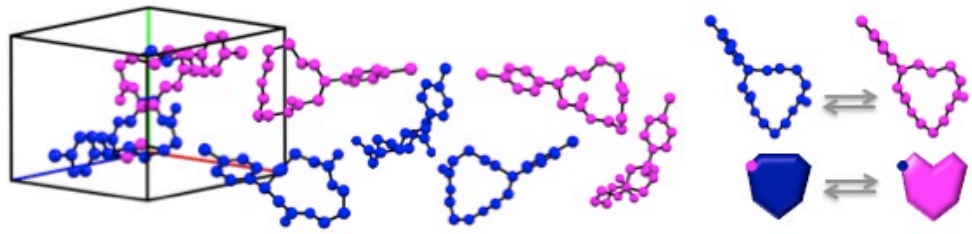

Abstract

The shapes adopted by large-ring, macrocyclic compounds play a role in their reactivity and their ability to be bound by biomolecules. We investigate the synthesis, conformational analysis, and properties of a specific family [13]-macrodilactones as models of natural product macrocycles. The features of our macrodilactones enable us to study the relationship between stereogenic centers and planar chirality through the modular synthesis of new members of this family of macrocycles. Here we report on insights gained from a new [13]-macrodilactone that is substituted at a position adjacent to the alkene in the molecule. Analysis of the compound, in comparison to an α-substituted regioisomer, by X-ray crystallography, NMR coupling constants, and reaction product characterization in concert with computational chemistry revealed that the alkene unit is dynamic. That is, the data support a model wherein the alkene in our [13]-macrodilactones is oscillating between two conformations. A difference in reactivity of one conformation compared to the other leads to manifestation of this dynamic behavior. The results underscore the local conformational dynamics observed in some natural product macrocycles, which could have implications for biomolecule binding.

Keywords

macrocycle conformation • conformational dynamics • density functional calculations • activation strain model

Introduction

Structural features that guide molecular conformations are important design elements underpinning the development of *de novo* bioactive macrocycles. Their utilization, though, requires an understanding of how a given feature actually influences conformations. Macrocycles have engendered enthusiasm as leads for drug development because they can be broken down into smaller domains that can modulate functions, affinity, specificity, and physicochemical properties.[1,2,3,4,5,6] Active compounds frequently fall outside of the typical rule of five parameters;[5] this has been rationalized by classifying macrocycles separately from other small molecules or by invoking the ability of specific macrocycles to adopt different conformations based on the local environment (e.g., dielectric of surrounding medium). This is because, among their special features, macrocycles balance domains that can make a molecule locally flexible while still being relatively rigid overall.[6,7,8] Macrocyclic conformations have been correlated with their bioactivity, particularly with respect to natural products and their analogs.[2,6,7,9,10] The point is not that a macrocycle limits the conformational space of a compound to only one conformation to thereby reap an enthalpic benefit upon binding. Rather, the macrocycle occupies a small number of low energy conformers, one of which will likely be the bound conformer. The ability to access multiple conformations likely assists in binding and also in tuning physical properties. As part of a project that aims to characterize the interplay between stereogenic centers at key positions of a model [13]-macrodilactone and the planar chirality of the ring, we have discovered that substitution on an allylic carbon modulates the dynamics of the ring between two inter-related conformers. Although discovered in the solid state, computation and solution experiments indicate that the interconversion, or "flutter", between conformations also occurs in solution.

A particular family of [13]-macrodilactones, typified by the macrocycle depicted in Figure 1, has provided a model system for the investigation of parameters that drive to the structure and conformation of macrocycles.[11,12,13,14] Several factors contribute to the rigidification of this family of macrocycles, primary among them are the two ester units and the alkene. The esters, for example, organize four ring atoms each. These atoms are the alkyl carbon, the ester oxygen, the carbonyl carbon, and the α-carbon (e.g., atoms 4-7 in Fig. 1). Four atoms are also rigidified in the case of the alkene (atoms 8-12). Twelve of the thirteen atoms in the macrocycle, therefore, are present in planar units. The connections between the planar units are of two varieties. A bond between the α-carbon of each ester and the corresponding allylic carbon on either end of the alkene unit constitutes one type of connection. Alternatively, the two esters are linked to each other via a bridging atom - the only atom of the macrocycle that is not involved in a planar unit. The planar units and their connectivity are intimately linked with the conformation adopted by the macrocycle.

The structure obtained from X-ray diffraction data for the unsubstituted [13]-macrodilactone is shown Figure 1c.[11b] Data from the solid state has been valuable to our understanding of how the functional groups and their connections translate into conformations in this family of macrocycles. The conformation of the macrocycle, dubbed the "ribbon" (*vide infra*), is shown with the alkene planar unit defining the top edge of a loosely triangle-shaped structure. The π-bond of the alkene is oriented perpendicular to the mean plane of the ring; consequently, one face of the alkene is pointing outwards and the other inwards. The ester units, with their carbonyls pointing in opposite directions, are the other edges of the triangle. The hinge atom allows them to twist relative to each other about an axis that goes through the center of the macrocyclic ring. The twisting of the planar units is handed. The chirality of the molecule, therefore, is based on the asymmetry of the wrapping of the ester arms around the double bond and is analogous to chirality of the enantiomers of (*E*)-cyclooctene. The structure shown in Figure 1 is only one, the p*S* enantiomer, of two (p*S* and p*R*) that are present in the crystal. Because the planar chirality is the only stereogenic element in the molecule, the macrocycle exists as a racemate.

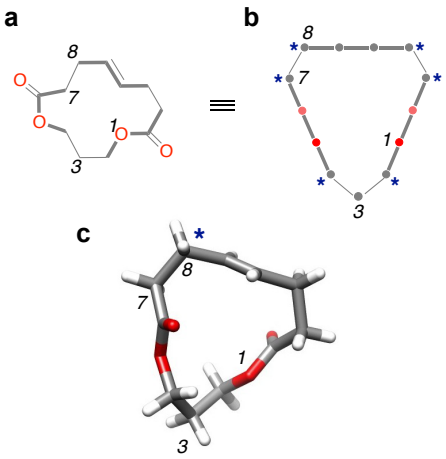

Figure 1. The [13]-macrodilactone motif as illustrated using the unsubstituted macrocycle. a) The connectivity of the ring. b) Schematic showing the three planar units and numbering of key atoms. c) Structure from X-ray crystallographic data; shown is the p*S* enantiomer of the racemate present in the crystal.

Our earliest investigations on the [13]-macrodilactones utilized chiral diol templates such as 4,6-*O*-acylated pyranose sugars.[12] Subsequently, we have identified several key atoms (i.e., C2, C4, C7, C12, in Fig. 1a,b) along the backbone of the macrocycle whose absolute stereochemistry will dictate the planar chirality of the macrocycle when there is only one substituent on the ring.[13,11] The commonality amongst these key centers is that they are at the terminus of a planar unit. Consider, for example, C4 and C7; these two atoms are at either end of one of the ester units of the [13]-macrodilactones. The interplay

between a point of asymmetry and a plane or axis of asymmetry is an important way to dictate the handedness of macrocycles and it has implications on the design of desired shapes for a particular application. The principle seems to be relatively general, with instances in both natural products and *de novo* compounds.[11b,15] Studies on other macrocycle motifs have shown that substitution at the allylic position could have either an effect on the overall conformation, or have no effect at all, like that of (-)-exiguolide and dictyostatin.[16,17] Since atoms C8 and C11 are at the termini of the alkene planar unit of our [13]-macrodilactone, we wanted to know if substitution there would similarly influence the planar chirality of the macrocycle, and consequently affect its low energy conformations. As with previous investigations on this macrocycle, we aimed to characterize the conformation in both the solid state and solution, and further understand what principles explain the observed conformations. The modularity of macrocycles, in terms of both their assembly[18] and conformational behavior[6,7] provided additional impetus for our investigation. Here we describe the synthesis and characterization of a new [13]-macrodilactone substituted at C8, the position β- to an ester carbonyl. Through a combination of spectroscopy, reactivity studies, and computational chemistry, a clearer picture of the low energy conformers of the macrocycle emerged. Further, potential energy surfaces for their interconversion and their epoxidation are also described.

Results and Discussion

Synthesis of [13]-macrodilactones substituted at the allylic carbon. Our established strategy for the synthesis of [13]-macrodilactones was used to prepare the new compounds used in this study. As depicted in Scheme 1, the acylation of known alcohol **1**[11a] with either 2-(*p*-bromophenyl)-4-pentenoic acid **2** or 3-(*p*-bromophenyl)-4-pentenoic acid **3** provides the respective ring closing metathesis (RCM) precursors, diene-diesters **4** and **5** in 79 and 74% yield, respectively. Substituted pentenoic acid **2** was prepared by alkylation of methyl *p*-bromophenylacetate,[19] whereas **3** was prepared from *p*-bromobenzaldehyde via a Johnson orthoester Claisen-based route.[20,21,22,23] With dienes **4** and **5** in hand, each one was converted to its corresponding [13]-macrodilactone by RCM to give **6** and **7** in 80 and 56% yield, respectively.

10.1002/asia.201700997

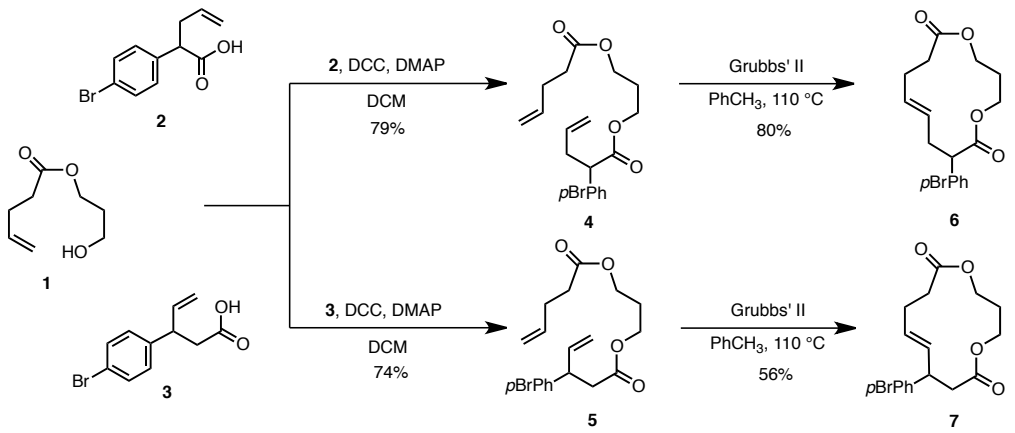

Scheme 1. Synthesis of [13]-macrodilactones **6** and **7**

S*olid state conformations of [13]-macrodilactone 7.* To our delight, [13]-macrodilactone **7** was a crystalline solid. We have previously relied on X-ray crystallography to understand how planar units and stereogenic centers at key centers affect the solid-state conformations of these macrocycles.[11,12,13] We expected that the carbon bearing the aryl ring was at the terminus of the alkene planar unit would guide the adoption of a ribbon conformation by the macrocyclic backbone as we had observed for other mono-substituted [13]-macrodilactones. Because **3** was racemic, we further anticipated that two complementary enantiomers would be in the unit cell for **7**; each configuration of the stereogenic carbon (*R* or *S*) would dictate the planar chirality (p*R* or p*S*) of the macrocycle. The X-ray structure of **7** we obtained, therefore, allowed us to compare it to our previously studied ring systems.

The unit cell of the crystals of **7** shows that the macrocycle took up the ribbon conformation as we had predicted based on the earlier compounds (Fig. 2). In this conformation were enantiomers of **7** where the configuration at C8 and the alkene were matched – the 8*R*,p*R* and the 8*S*,p*S* isomers. The planar chirality of these conformers was guided by the configuration at the key C8 atom, as expected. What was not anticipated, though, was to find an additional pair of macrocycle conformers in the same unit cell. This new conformer was characterized by a partial rotation of the alkene unit (C8-C11) that switches its planar chirality for a given stereogenic center. The consequence of the partial bond rotation formally converts the 8*R*,p*R* ribbon conformer to the 8*R*,p*S* and similarly the 8*S*,p*S* becomes 8*S*,p*R*. When the new conformer is viewed from the (planar) axis of chirality, a kink in the backbone is apparent (Fig. 2a); we dub this the "heart" conformer based on its resemblance to a cartoon heart. A conformational map in Figure 2b graphically illustrates the alkene shifting from p*S* to p*R* planar chirality for the 8*R* isomer of **7**. The unit cell is populated by a 1:1 mixture of the two macrocycle conformers, as well as their corresponding enantiomers. Figure 2c is a stylized version of the unit cell that shows both the conformers. Additional copies of C9 and C10 for each conformer demonstrate that the sites within

the unit cell are degenerate – any of the four conformers can be present in a given spot. It became apparent that the conformations observed in the crystal structure were also likely to be present in solution. Efforts to get information about solution conformations of **7** were therefore undertaken.

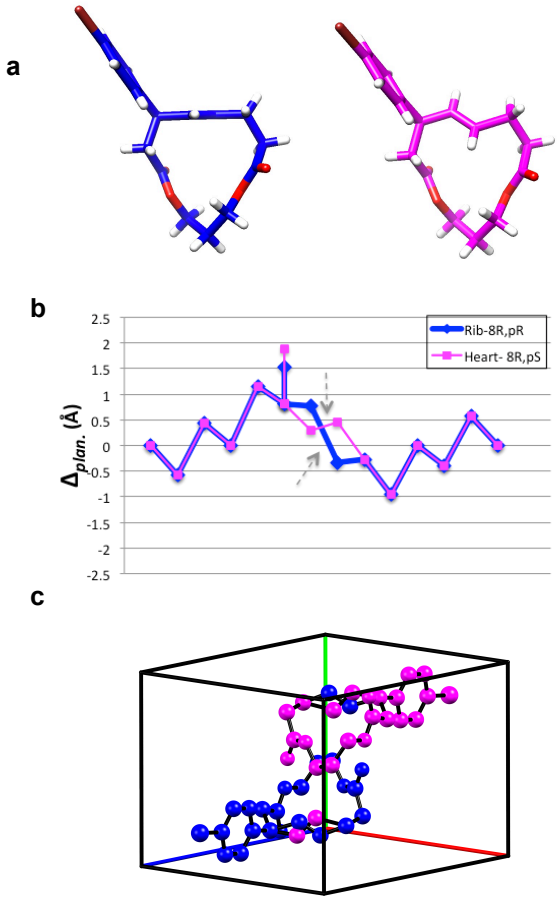

Figure 2. (a) Ribbon (blue) and heart (pink) conformers of 8*R* configured **7**. (b) A conformational map displaying a visual difference of the alkene in the ribbon (8*R*,p*R*) and heart (8*R*,p*S*) conformers; blue represents the ribbon, while pink represents the heart. Dashed arrows indicate the orientation of the C9-C10 (alkene) bond in each conformer. (c) Unit cell showing the skeletal versions of both the ribbon (8*S*, p*S*) and heart (8*R*, p*S*) conformers being present. Enantiomers of each were omitted (8*R*, p*R* for ribbon and 8*S*, p*R* for heart), for visual purposes, but all four isomers do exist in the unit cell.

*Solution conformations of **6** and **7** by NMR and molecular modeling.* Since the crystal structures of previously synthesized [13]-macrodilactones led us to believe that there was only the ribbon conformer present in the unit cell, we decided to investigate two macrocycles: **7** as the test system and **6** as a control. A strategy that leveraged NMR data in conjunction with quantum chemical conformational energies was adopted to gain a better understanding of the behavior of **7** in solution. Versions of this same strategy are well precedented for macrocycle conformational analysis.[24,25] Coupling constants predictably play an important role in the technique. Guided by the crystal structure data for **7**, we opted

to focus on ^{3}Js in the region of the molecule where the change in conformation was most pronounced between the ribbon and heart conformers. Specifically, the alkene and the surrounding carbons from the carbonyl carbon C6 to carbonyl C13 (**I** in Scheme 2), partially flipped over the course of the transition. This rotation had a significant effect on several dihedral angles between atoms in this part of the macrocycle.[26] By using both **6** and **7**, then, it was expected that ^{1}H signals for the allylic (C8, C11) and alkenyl protons (C9, C10) would harbor important coupling constants. The appearance of the ^{1}H NMR spectrum suggested that average signals were being observed and that the two conformers, if both present, were not in slow exchange. Table 1 organizes coupling constants collected from NMR data for the allylic and alkenyl protons. Couplings are depicted with double-headed arrows in the table. Experimental values were compared to those calculated with a Karplus equation[27] and density functional theory (DFT) calculations at the ZORA-B3LYP/QZ4P//BLYP-D3(BJ)/TZ2P level. These couplings provided important information about dihedral angles in this fragment of the molecule. The calculated coupling constants were based on low energy conformations that were likely to be the primary contributors to the overall ensemble of conformers available in solution.

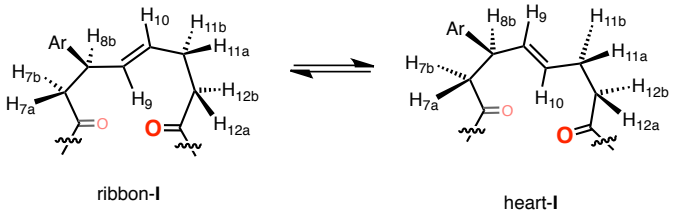

Scheme 2. Rendition of the C6-C13 fragment (**I**) of **7**

Table 1. Select $^{3}J_{H,H}$ values (Hz) for compounds **6** and **7**

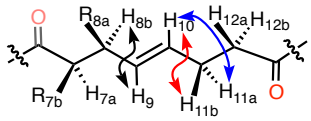

^{3}J coupling	obs.	Karplus rib.	Karplus *hrt.*	DFT rib.	DFT *hrt.*
compound **7**					
H_{10}-C_{10}-C_{11}-H_{11a}	10.4	11.35 170.5°	3.02 -71.19°	11.39	3.57
H_{10}-C_{10}-C_{11}-H_{11b}	7.6	4.06 52.84°	11.28 169.2°	4.72	12.10
H_{8b}-C_{8}-C_{9}-H_{9}	7.8	11.44 172.3°	4.76 42.73°	11.40	4.50
compound **6**					
H_{8b}-C_{8}-C_{9}-H_{9}	8.7	10.79 162.5°	-	11.27	4.54
H_{10}-C_{10}-C_{11}-H_{11a}	9.6	10.89 163.7°	-	11.60	3.15

The observed $^{3}J_{H,H}$ values in Table 1 were collected in a multi-step process and provided values that could be compared to Karplus computed and DFT calculated coupling constants. Signals of the ^{1}H NMR spectra were assigned for **6** and **7** from spectra collected in both $CDCl_3$ and C_6D_6. Deutero-benzene (C_6D_6) gave better overall dispersion of signals but some from the $CDCl_3$ spectra were resolved where there was overlap in the C_6D_6 spectra. Due to the similarity of the dielectric constants of both solvents, we used data from each spectrum interchangeably. Three main H-H relationships were used to characterize the conformers of macrocycle **7** in solution: H10-H11a, H10-H11b, and H8-H9b . The H10-H11a ^{3}J has an observed value of 10.4 Hz, which is closer to the computed/calculated ribbon value for this dihedral than to the heart conformer (~11 Hz for ribbon versus ~3.5 Hz for heart). On the other hand, both the H10-H11b ^{3}J (7.6 Hz) and the H8-H9b ^{3}J (7.8 Hz) are between the values calculated for the ribbon and heart conformations. In fact, they are nearly the average value between the two (The average values would be 8.4 and 7.9 Hz, respectively.), suggesting that there may be equal populations of both conformers in solution. The H10-H11a and H8-H9b ^{3}J values for compound **6** gave similar information about the conformations of this macrocycle. The H10-H11a displays a coupling constant of 9.6 Hz in NMR, a value between the average of the two conformers (7.38 Hz) and the ribbon computational value (11.60 Hz). Also, the ^{3}J of H8-H9b is 8.7 Hz, which is also intermediate between the values for the ribbon and heart conformers. The data are interpreted as an indication of a dynamic conformational profile for this segment of the molecule for both **6** and **7**. Values of several C-H ^{3}Js were also evaluated for macrocycles **6** and **7**.[26] There was less agreement between the measured, computed, and calculated values for these coupling constants, however. Part of the reason behind the discrepancies may be related to the measurement of the values themselves. The difficulty stemmed from the overlap of signals that prevented the accurate measurements, even at high field (700 MHz). Consequently, they did not provide us sufficient confidence about the conformations of the macrocycles to be interpretable.

Although the NMR solution study suggested that the ribbon and heart conformers were populated for *both* macrocycles, the data were at least partially equivocal. Computational studies were carried out, therefore, in order to better understand the conformational preferences of **6** and **7**. Using density functional calculations, we calculated the potential energy surfaces (PES) associated with isomerization of the 7*S* enantiomer of **6** and the 8*R* enantiomer of **7** (Fig. 3). The rationale was that the absolute configuration of each position (7*S* and 8*R*) corresponded to the *R* configured planar chirality. We had previously shown that the configuration of key atoms dictates the planar chirality associated with the [13]-macrodilactones. Figure 3 places the heart conformers on the left-hand side, the ribbons on the right-hand side, and the structure associated with the transition state between the two. It should be

noted that when the alkene unit of each macrocycle flips, the planar configuration also flips (i.e from p*R* to p*S*).

Inspection of the PES of **7** reveals that at ambient temperature, the two conformers, heart **7** and ribbon **7**, are of similar energies with the overall exergonicity associated with the formation of the ribbon structure from the heart being small, (ΔG_{rxn} = –1.9 and –0.4 kcal/mol in gas phase and toluene, respectively). This result is consistent with the idea that the heart and ribbon conformers can exist in both solid state and solution, likely to a similar extent. Further, there is a nominal barrier of inversion around the double bond of 3.9 and 4.4 kcal/mol in the gas phase and toluene, respectively. The vinylic CHs of the alkene in the ribbon conformation are orthogonal to the plane of the ring, while in the heart conformation they are in the plane (H-C9 out of the ring H-C10 inside the ring). The transition states involved in conversion between heart and ribbon shapes of both **6** and **7** were located by scanning the potential energy surface associated with rotation of the vinylic CH with respect to the plane of the macrocycle. Starting from the heart shape, this motion can be thought of as the H-C10 moving through the center of the ring. Rotation in the opposite direction is energetically unfavorable and requires more degrees of rotation.

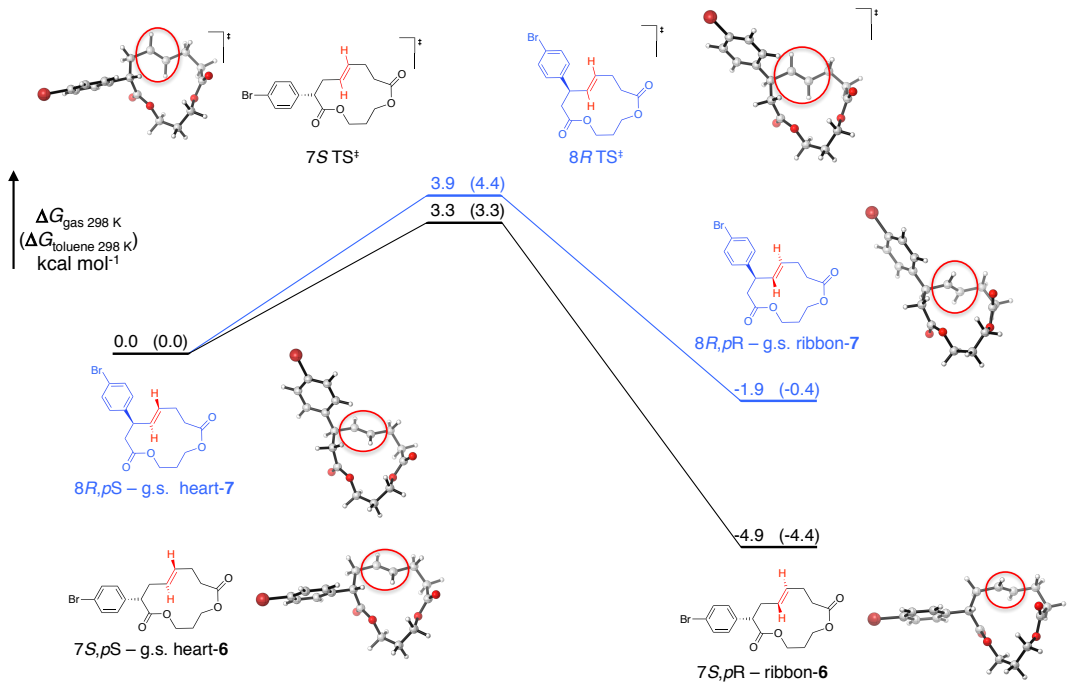

Figure 3. Computed reaction profiles (Δ*G*) for the isomerization between the ribbon and heart shaped macrocycles **6** and **7.** All data were computed at the BLYP-D3(BJ)/TZ2P level in the gas phase and in toluene with relative energies in kcal/mol.

Analysis of the PES for isomerization of **6** reveals key similarities and differences with respect to the PES of **7**. First, the barrier of isomerization is slightly less than for **7**, although it is more or less the same. The reaction in toluene is exergonic by –4.4 kcal/mol, with the reverse barrier increasing to 7.7 kcal/mol. Taken together, it is reasonable that, while ribbon **6** is 4 kcal/mol more stable that ribbon **7**, there is a relatively low barrier associated to interconversion between ribbon and heart conformers for both of them. The fact that the heart conformer of **6** is not observed in the crystal structure of related α-substituted [13]-macrodilactones[11b] may simply be related to crystal packing forces.

What remained necessary was to put our observations into the context of a physical model that could rationalize the conformations and the dynamics of the [13]-macrodilactones. Specifically, we wanted to explain why, in the case of **7**, both the ribbon and the heart conformers were adopted in nearly equal populations. The main difference between the two conformers is in the orientation of the double bond. Both have the aryl ring in a pseudo-equatorial disposition relative to the macrocycle, likely to minimize transannular interactions. The rotamer about the C-aryl, C8 bond, present in the crystal structure and computational structures, puts the aryl ring in an eclipsing orientation relative to the benzylic CH ("aryl parallel"). This has been shown to be the preferred rotamer for equatorial aryl groups in cyclohexanes,[28] 1,3-dioxanes, and tetrahydropyrans.[29] In the six membered-ring cases this preference is adopted because steric interactions between ortho-hydrogens of the aryl ring and equatorial hydrogens on the saturated ring are avoided. It is likely that a similar effect is at play for the [13]-macrodilactones. The benzylic carbon in **7** is flanked by a saturated methylene on the one side (the carbon α– to the ester carbonyl, C7) and a vinyl group on the other. The ortho hydrogen of the aryl ring is some distance from the pseudo-equatorial hydrogen of the methylene (3.118 Å) but it is close to the proximal vinyl proton (2.482 Å). In the heart conformation, the proximal vinyl is significantly farther away from the ortho hydrogen (3.948 Å). The main driver between this subtle difference in conformations is, therefore, this steric interaction. While it is speculative, the close proximity and geometry of a vinylic CH bond to the carbonyl oxygen of an ester in the heart conformation is also noteworthy. One thing that becomes clear from the analysis of the solid state and computational structures of both **6** and **7**, though, is that the conformational dynamics are primarily localized around the alkene portion of the molecule. It does not seem that the other planar units (the two esters) are oscillating in a similar way.

Macrocyclic diastereocontrol as a readout of solution conformations. In an attempt to better understand the solution conformations of the [13]-macrodilactones, epoxidation reactions were performed. There is no internal cavity of the [13]-macrodilactones so, based on the planar chirality, only one face – the outer face of the alkene is available to react with electrophiles. The planar chirality of the ring, therefore, controls the diastereoselectivity of epoxidation of the [13]-macrodilactones, which is an

10.1002/asia.201700997

example of macrocyclic diastereocontrol.[30] Macrocycles **6** and **7** were both epoxidized under established reaction conditions that involved either *in situ* generation of dimethyl dioxirane (DMDO) in the presence of the substrate or addition of a solution of DMDO to a solution of the substrate.[10,31] When α-substituted [13]-macrodilactone **6** was the substrate, two diastereomeric epoxides, **9** and **10** (Fig. 4), were obtained in an approximately 1:3 ratio. This result initially seemed inconsistent with results obtained of epoxidation on the related compound, α-phenyl substituted [13]-macrodilactone **8**.[11b] When the reaction was revisited, however, we found that **8** does, in fact, provide two diastereomeric epoxide products in an approximately 1:3 ratio (**11**:**12**). These results suggest that both sides of the alkene are reacting. A model where reaction occurs through both the heart and the ribbon conformations is consistent with, or even required by, the observed products. Epoxidation of β-substituted macrodilactone **7** was also conducted; in this case, two products that we ascribe as diastereomeric epoxides **13** and **14** came about in an approximately 1:7 ratio. Upon initial consideration, an explanation for these results was not obvious so we once again resorted to computational chemistry in the hope of gaining insight into the reaction.

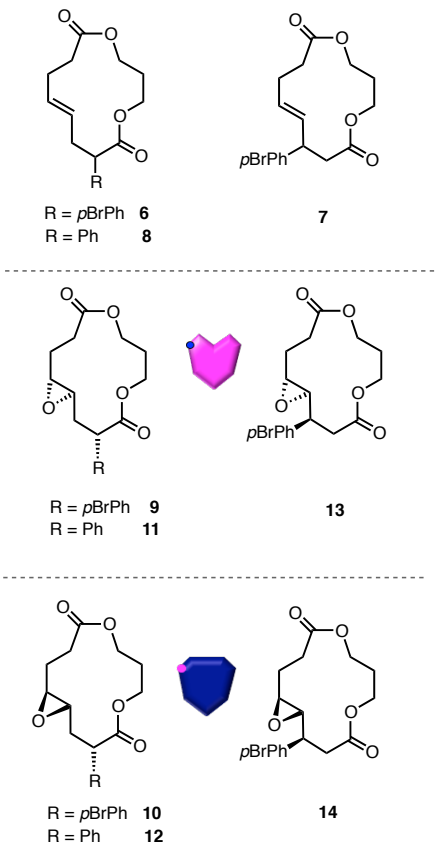

Figure 4. [13]-Macrodilactones **6-8** and the products of their epoxidation, organized by the conformer that gives rise to each diastereomer: **9**, **11**, **13** are the major isomers via the heart conformers; **10**, **12**, and **14** are the minor isomers via the ribbon.

The objective of the computational investigation was to determine whether the observed epoxide product distributions could be qualitatively rationalized when considering the conformational equilibria of macrocycles **6** and **7** and the transition states associated with each. Toward that goal, the stationary points on the potential energy surface (PES) for the DMDO mediated epoxidation of **6** and **7** were found. Extensive conformational searches for transition states have been conducted, and only the lowest energy conformers are shown in this work. Even though the ring closing metathesis reaction is carried out in toluene, when the macrocycle is epoxidized in DCM, the equilibrium between the two topologies (ribbon and heart) will be shifted and we then computed the entire PES, that is, isomerization as well as epoxidation, in DCM. The α- and β-substituted *p*-Br macrocycles **6** and **7** were re-optimized in both the ribbon and the heart conformations in DCM, the new solvent. These conformers served as the starting point for modeling the epoxidation reaction. At this point the transition state (TS) was located using initial structures derived from Houk's and Jorgensen's published coordinates, which involved epoxidation of *cis*- and *trans*-2-butene by DMDO.[32] Moving along the reaction coordinate, the final epoxide product was then also located. During the epoxidation, DMDO is converted to acetone. Computed energies that represent the PES of isomerization and epoxidation in DCM for macrocycles **6** and **7** are collected in Table 2; figures showing the PES for each compound are provided in the Supporting Information.

Table 2. Computed reaction energies (kcal/mol) for the isomerization between the ribbon and heart conformers of **6** and **7** and epoxidation reactions leading to adducts **11 - 14**.[a]

	conformer/compound	Energy (kcal/mol) α	Energy (kcal/mol) β	conformer/compound	
heart	7*S*,p*S* – epoxide (**11**)	-53.3	-53.4	8*R*,p*S* – epoxide (**13**)	*heart*
	7*S*,p*S* – epoxidation TS‡	13.9	13.5	8*R*,p*S* – epoxidation TS‡	
	7*S*,p*S* – g.s. heart-**6**	0.0	0.0	8*R*,p*S* – g.s. heart-**7**	
	7*S* TS‡ (**6**)	5.7	4.1	8*R* TS‡ (**7**)	
	7*S*,p*R* – g.s. ribbon-**6**	-1.1	-0.5	8*R*,p*R* – g.s. ribbon-**7**	
ribbon	7*S*,p*R* – epoxidation TS‡	10.7	8.5	8*R*,p*R* – epoxidation TS‡	**ribbon**
	7*S*,p*R* – epoxide (**12**)	-58.9	-58.4	8*R*,p*R* – epoxide (**14**)	

[a] Computed at the BLYP-D3(BJ)/TZ2P level in DCM.

A number of observations become apparent when considering the relative energetic values in Table 2. First, the isomerization of ground state macrocycles between heart and ribbon conformers in DCM is reminiscent of the surface calculated in toluene earlier. The ribbon conformers for both **6** and **7** are preferred, and that preference is more pronounced (by 0.6 kcal/mol) for α-substituted macrocycle **6**.

10.1002/asia.201700997

Similarly, conversion from the ribbon to the heart conformer requires 6.8 and 4.6 kcal/mol for **6** and **7**, respectively. This suggests that interconversion of the conformers occurs readily under the reaction conditions. Second, the products that are the result of epoxidation of the ribbon conformer are more stable (by ~5 kcal/mol) than those that arise from the heart conformer. Third, activation barriers for epoxidation of the heart conformers are higher in both cases compared to the ribbon conformers. Epoxidation of the ribbon conformer of **6** and **7** is the preferred pathway in terms of energetics and, based on the Curtin-Hammett Principle, should deliver the major product diastereomer. Amongst the four transition states, the one with ribbon configured, 8*R*,p*R* β-macrocycle **7** and DMDO is the most stable at 8.5 kcal/mol relative to reactants. Fourth, the barrier for epoxidation of the 7*S*,p*S* heart structure of α-macrocycle **6** is 2.1 kcal/mol higher than that of the 7*S*,p*R* ribbon. For **7** the 8*R*,p*S* heart is 4.4 kcal/mol higher than the 8*R*,p*R* ribbon. There is a greater preference, therefore, for epoxidation of **7** to proceed via the ribbon conformer than there is for **6**. There is strong qualitative agreement, therefore, between the picture painted by the analysis of the PES and the higher diastereoselectivity in epoxidation of β-macrocycle **7**.

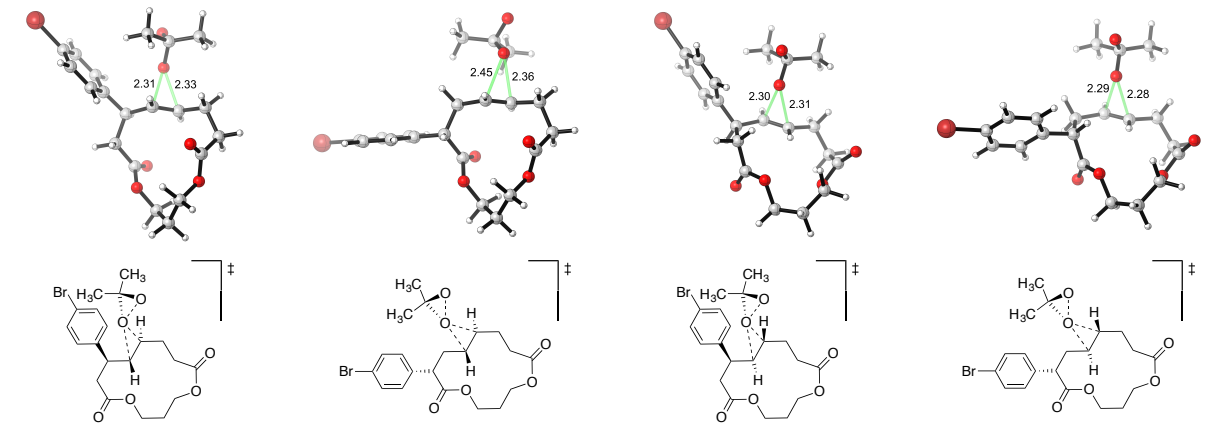

Figure 5. Structures (in Å) of the TSs and relative activation free energies $\Delta\Delta G^{\ddagger}_{DCM,298K}$ (in kcal/mol) computed at the BLYP-D3(BJ)/TZ2P level.

Inspection of the geometries and associated energies of the transition states in the epoxidation reaction reveals additional insights. The computed TS geometries confirmed that epoxidation is a concerted asynchronous process; that is, the newly forming C–O bond distances are not equal. The extreme case being for 7*S*,p*R* ribbon, where the difference in bond distance is 0.9 Å. This is at variance with the previous accounts on the very simple model reaction involving (*E*/*Z*)-but-2-ene.[32] Apparently,

the *p*-bromophenyl group and other geometric features in the [13]-macrodilactones prohibit a synchronous process.

Next, the activation strain model (ASM),[33] also known as the distortion/interaction model[34] was applied to understand the factors giving rise to the activation barriers associated with the epoxidation reaction in the gas phase. This analysis is based on the "electronic energy (*E*)" that constitutes the multidimensional PES of a system and thus its state function, which determines all thermal and statistical effects leading to *H* or *G*. The activation barrier results from the interplay between the strain ΔE_{strain} and interaction ΔE_{int} energies, as shown in Equation 1:

$$\Delta E^{\ddagger} = \Delta E^{\ddagger}_{strain} + \Delta E^{\ddagger}_{int} \quad (1)$$

In this framework, each transition state structure is separated into two fragments, namely the distorted macrocycle and the distorted DMDO, followed by single-point energy calculations on each fragment. The difference in energy between the optimized energy minimum structure for a given species and geometry it adopts in the transition state is the strain, $\Delta E^{\ddagger}_{strain}$, while the $\Delta E^{\ddagger}_{int}$ is the interaction between the deformed reactants.

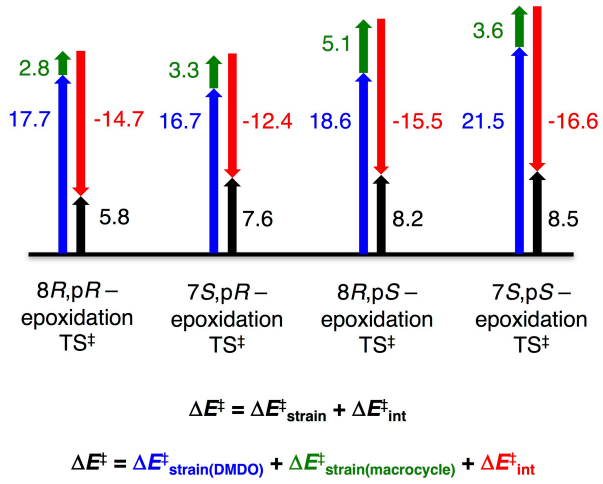

Figure 6. Graph of interaction, strain, and activation energies for the epoxidation reactions of ribbon **6**, heart **6**, ribbon **7**, and heart **7**. Energies (in kcal/mol) computed at the BLYP-D3(BJ)/TZ2P level in the gas phase.

It is difficult to attribute the difference in reactivity between the different conformations of the macrocycle to either the $\Delta E^{\ddagger}_{strain}$ or the $\Delta E^{\ddagger}_{int}$ exclusively. Trends, however, do emerge and from Figure 6. The total strain energy, for example, is primarily due to distortion of the DMDO molecule. Furthermore, we find that the strain associated with epoxidation of the ribbon macrocycles is lower

compared to that of the heart macrocycles ($\Delta\Delta E^{\ddagger}_{strain}$ = 3.2 – 4.5 kcal/mol). This, along with a favorable interaction, leads to markedly lower barriers for epoxidation of the ribbon macrocycles. Comparison of the ribbon conformers reveals that the $\Delta E^{\ddagger}_{strain}$ term is nearly equivalent, but the more favorable interaction for the ribbon **7** leads to a lower barrier ($\Delta\Delta E^{\ddagger}$ = 1.8 kcal/mol). Additionally, we see that the greater distortion energies associated with epoxidation of the heart shaped macrocycles overtakes their more favorable interaction energies, thereby resulting in higher activation barriers compared to the ribbon conformations.

Conclusion

The main insight gained from this project is that the *p*-bromophenyl substituent at the allylic position (C8) of our [13]-macrodilactone motif engenders flexibility in the macrocycle that is observable in both the solid state and in solution. Two essentially equi-energetic conformers, the ribbon and the heart, are populated by compound **7**. This conformational effect is in contrast to other studies on natural product macrocycles where an allylic substituent either had little effect on the conformational dynamics or it helped to rigidify it. The results also support the contention that the flexibility is a local effect. That is, of the two esters and the alkene units in the macrocycle, it is only the alkene moiety that shows evidence of fluctuating. Epoxidation reactions of the alkene unit revealed additional differences between C7 and C8 substituted [13]-macrodilactones. Specifically, there was a greater difference in the transition state energies for the ribbon and heart conformers for **7** than there was for a-substituted macrocycle **6**. The consequence was that **7** showed a qualitatively higher macrocyclic diastereoselectivity. Throughout the experimental investigation, computational chemistry guided the explanation of our observations. This fact underscores the significant impact that computational chemistry had on the project. Finally, the conformational and reactivity patterns observed underscore the natural product-like properties of this family of [13]-macrodilactones.

Experimental

General Synthetic Methods

Unless stated otherwise, all acylations were conducted at 0 °C and then left overnight (~10 h) at room temperature (rt). Reactions were monitored using TLC. UV light and $KMnO_4$ or Ceric Ammonium Molybdate (CAM) solution were used for visualization. Chromatography was performed on silica gel and solvent systems were based on the R_f values. The ^{1}H NMR spectra collected were referenced to

$CDCl_3$ (δ_H 7.27 ppm) or C_6D6 (δ_H 7.16 ppm) at 400 MHz. 500 MHz, and 700 MHz. ^{13}C NMR spectra collected at 100 MHz were referenced to $CDCl_3$ (δ_C 77.2 ppm) or C_6D_6 (δ_C 128.4 ppm).

General Method for the Acylation of Monoester 1

Dicyclohexyl carbodiimide (DCC) (1.08 eq) and dimethylaminopyridine (DMAP) (0.5 eq) were added in DCM (8 mL) and cooled to 0 °C. The acid of choice (0.78 mmol, 1.0 eq), i.e., either **2** or **3** (See SI for synthetic details of **2**[19] and **3**[20,21,22]), was added to the solution and stirred for 30 minutes. Monoester **1** (0.78 mmol, 1 eq) was added to the mixture as a solution in DCM (2 mL) and the mixture was stirred overnight at rt. The mixture was then filtered through a short pad of celite to remove dicyclohexyl urea (DCU) that had partially precipitated from the solution. The pad was washed with an additional portion of Et_2O (5 mL). The solvents were removed from the filtrate under reduced pressure and the residue was taken up in cold Et_2O (10 mL). Additional DCU was filtered off through a short pad of celite after additional washes with cold Et_2O (2 x 2 mL) and the combined filtrates were concentrated under reduced pressure. The residue was purified by silica gel column chromatography to give the corresponding diene-diesters.

Compound 4: This compound was prepared using the general acylation method of **1** with acid **2** to give compound **4** in 79% yield and as a colorless oil. R_f 0.44 (Hexanes: EtOAc 90:10); ^1H NMR ($CDCl_3$) 400 MHz δ 7.41 (d, 2H, *J*= 8.6 Hz), 7.15 (d, 2H, *J*= 8.6 Hz), 5.71 (m, 2H), 5.01 (m, 3H), 4.94 (dd, 1H, *J*= 4.7, 1Hz), 4.11 (ddd, 2H, *J*= 11.3, 11.3, 4.8 Hz), 4.04 (ddd, 2H, *J*= 6.3, 6.3 Hz), 3.58 (dd, 1H, *J*= 7.9, 7.9 Hz), 2.74 (ddd, 1H, *J*= 14.7, 7.9, 7.9 Hz), 2.46 (ddd, 1H, *J*= 13.8, 6.9, 6.9 Hz), 2.33 (m, 4H), 1.87 (p, 2H, *J*= 6.3 Hz); ^{13}C NMR ($CDCl_3$) 100 MHz δ 172.8, 137.4, 136.6, 134.7, 131.7, 129.7, 121.3, 117.4, 115.5, 61.5, 60.7, 50.8, 37.3, 33.4, 28.8, 27.9; TOF HRMS *m/z* calcd for $C_{19}H_{24}O_4Br$ $[M+H]^+$ 395.0858, found 395.0845.

Compound 5: This compound was prepared using the general acylation method of **1** with **3** to give compound **5** in 74% yield and as a colorless oil. R_f 0.43 (Hexanes: EtOAc 90:10); ^1H NMR ($CDCl_3$) 400 MHz δ 7.43 (d, 2H, *J* = 8.3 Hz), 7.10 (d, 2H, *J* = 8.3 Hz), 5.93 (ddd, 1H, *J* = 17.2, 10.4, 6.8 Hz), 5.82 (ddd or dt, 1H, *J* = 10.4, 10.4, 4.6 Hz), 5.09 (d, 2H, *J* = 7.8 Hz), 5.01 (d, 2H, *J* = 10.9 Hz), 4.08 (ddd, 4H, *J* = 6.2, 6.2, 6.2 Hz), 3.83 (ddd, 1H, *J* = 7.5, 7.5, 7.5 Hz), 2.72 (dddd or dq, 2H, *J* = 15.3, 15.3, 15.3, 7.8 Hz), 2.40 (ddd, 4H, *J* = 15.0 11.0, 4.3 Hz), 1.88 (ddd or dt, 2H, *J* = 12.4, 6.2, 6.2 Hz); ^{13}C NMR ($CDCl_3$) 100 MHz δ 173.1, 171.6, 141.5, 139.9, 136.8, 131.9, 129.5, 115.8, 115.5, 61.3, 61.0, 53.6, 45.2, 40.2, 33.7, 29.0, 28.2; TOF HRMS *m/z* calcd for $C_{19}H_{24}O_4Br$ $[M+H]^+$ 395.0858, found 395.0827.

General Ring Closing Metathesis (RCM) Procedure

In a dry round bottom flask under an atmosphere of N_2 was added a solution of the diene (either **4** or **5**, 1.06 mmol) in freshly distilled toluene so that the diene concentration was 5 mM. To the solution was

added, as a solid, either Grubbs' second-generation catalyst or Hoveyda-Grubbs' second generation catalyst (10 mol%). The round bottom was fitted with a reflux condenser, under N_2, and the mixture was heated to 110 °C for 18 h. After, the toluene was removed under reduced pressure to give a residue that was then purified by column chromatography.

Compound 6: The synthesis followed the general RCM method using Grubbs' second generation catalyst with compound **4** to give [13]-macrodilactone **6** in a 80% yield as a white powder. m.p 108.8-111.0 °C; R_f 0.45 (Hexanes: EtOAc 80:20); ^{1}H NMR (C_6D_6) 500 MHz δ 7.21 (d, 2H, *J* = 8.3), 7.01 (d, 2H, *J* = 8.3), 5.43 (m, 2H), 4.44 (m, 1H), 4.35 (m, 1H), 3.65 (ddd or dt, 1H, *J* = 11.4, 3.9, 3.9), 3.36 (m, 2H), 2.69 (ddd or dt, 1H, *J* =12.9, 12.9, 8.7), 2.27 (dddd, 1H, *J* = 18.0, 9.6, 9.6, 3.1), 2.06 (m, 1H), 2.03 (m, 1H), 1.95 (m, 2H), 1.36 (m, 2H); ^{13}C NMR (C_6D_6) 100 MHz δ 173.5, 173.1, 138.7, 132.3, 131.8, 130.1, 129.2, 122.0, 60.9, 60.3, 52.9, 38.5, 34.4, 29.1, 26.6; TOF HRMS *m/z* calcd for $C_{17}H_{19}O_4Br$ $[M+H]^+$ 367.0545, found. 367.0545.

Compound 7: Compound **7** was prepared using the general RCM method on diene **5** with Hoveyda-Grubbs' second-generation catalyst to give the product in 56% yield as a white crystalline solid. m.p. 115.3-116.8 °C; R_f 0.38 (Hexanes: EtOAc 80:20); ^{1}H NMR (C_6D_6) 500 MHz δ 7.18 (d, 2H, *J* = 8.7 Hz), 6.53 (d, 2H, *J* = 8.3), 5.39 (m, 2H), 4.38 (ddd, 2H, *J* = 11.0, 11.0, 6.2), 3.69 (ddd, 1H, *J* = 15.3, 4.1, 4.1), 3.65 (ddd, 1H, *J* = 15.0, 4.1, 4.1), 3.60 (ddd or dt, 1H, *J* = 11.1, 4.2, 4.2), 2.37 (dd, 1H, *J* = 13.3, 12.4), 2.26 (dd, 1H, *J* = 13.6, 3.1), 2.20 (dddd, 1H, *J* = 10.6, 7.6, 5.0, 2.9), 2.06 (ddd, 1H, *J* = 13.8, 7.1, 3.2), 1.99 (ddd, 1H, *J* = 13.9, 10.9, 3.0), 1.87 (dddd, 1H, *J* = 13.9, 10.5, 7.0, 3.4), 1.43 (m, 2H); ^{13}C NMR (C_6D_6) 100 MHz δ 173.0, 171.2, 142.8, 133.7, 132.3, 130.2, 129.5, 121.0, 60.9, 60.6, 46.2, 41.6, 34.4, 28.9, 26.3; TOF HRMS *m/z* calcd for $C_{17}H_{20}O_4Br$ $[M+H]^+$ 367.0545, found 367.0531.

DMDO general procedure for epoxidation of macrocycle 6 and 7

At rt in a dry vial containing 4 Å mol. sieves and a stir bar, the macrocyclic substrate (0.109 mmol, 1.0 eq.) was dissolved in dry DCM (0.1 mL) and parafilmed with a septum. To this solution was then added DMDO[31] in DCM (3 mL, 0.094 M, 2.5 eq) via a syringe. The mixture was stirred for 3 h and then the solvents were removed under reduced pressure and the mixture was analyzed by NMR.

Compound 9 and 10: Compounds **9** and **10** were prepared using the general procedure for epoxidation of macrocycles. The products, as a 1:3 mixture of diastereomers, were analyzed without separation. R_f 0.27, 0.19 (hexanes: EtOAc 80:20); ^{1}HNMR ($CDCl_3$) 400 MHz δ 7.44 (d, 7H, *J*= 8.3 Hz), 7.19 (d, 2H, *J*= 7.8 Hz), 7.15 (d, 5H, *J*= 8.1), 4.77 (m, 5H), 4.60 (ddd, 1H, *J*= 11.5, 8.2, 3.0 Hz), 4.48 (ddd, 1H, *J*= 12.1, 9.6, 3.3 Hz), 4.21 (ddd, 1H, *J*=9.0, 5.4, 3.6 Hz), 3.97 (m, 1H), 3.91 (m, 2.5H), 3.69 (m, 5H), 3.51 (m, 1H), 2.99 (m, 1H), 2.84 (m, 7H), 2.46 (m, 7H), 2.25 (m, 5H), 2.05 (m, 7H), 1.95 (m, 3H), 1.68 (m, 1H), 1.58 (m, 3H), 1.46 (m, 1H); ^{13}C NMR ($CDCl_3$) 100 MHz δ 173.1, 173.0, 172.8, 138.0, 137.5,

132.2, 132.1, 129.5, 129.3, 121.8, 64.6, 64.0, 60.4, 59.5, 58.5, 57.4, 56.6, 55.8, 48.3, 47.2, 36.5, 36.3, 30.1, 29.6, 28.1, 26.9, 26.5, 26.3; TOF HRMS *m/z* calcd for $C_{17}H_{20}O_5Br$ $[M+H]^+$ 383.0494, found 383.0484.

Compound 13 and 14: Compounds **13** and **14** were prepared using the general procedure for epoxidation of macrocycles. The products, as a 1:7 mixture of diastereomers, were analyzed without separation. R_f 0.24, 0.16 (hexanes: EtOAc 80:20); ^{1}HNMR ($CDCl_3$) 400 MHz δ 7.46 (d, 14H, *J* = 8.5 Hz), 7.15 (d, 14H, *J* = 8.2 Hz), 4.80 (m, 14H), 4.44 (ddd or dt, 1H, *J*= 11.4, 5.2, 5.2 Hz), 4.32 (m, 2H), 4.23 (ddd, 1H, *J*= 11.7, 5.4, 5.4Hz) 3.96 (ddd, 7H, *J* = 8.26, 4.3, 4.3 Hz), 3.86 (ddd, 7H, *J* = 7.4, 3.7, 3.7 Hz), 3.61 (ddd, 1H, *J*= 11.2, 3.1, 3.1 Hz), 3.04 (dd, 1H, *J*= 2.5, 2.5 Hz), 2.99 (m, 8H), 2.76-2.89 (m, 21H), 2.60 (m, 8H), 2.43 (m, 16H), 2.23 (m, 8H), 2.13 (m, 2H), 2.08 (m, 14H), 1.55 (m, 11H); ^{13}C NMR ($CDCl_3$) 100 MHz δ 172.8, 171.6, 140.4, 132.0, 131.9, 129.8, 129.3, 121.2, 63.8, 63.6, 61.9, 60.4, 59.9, 59.1, 54.6, 43.6, 37.1, 29.9, 29.6, 27.3, 27.0, 26.9, 26.7; TOF HRMS *m/z* calcd for $C_{17}H_{20}O_5Br$ $[M+H]^+$ 383.0494, found 383.0477.

Computational Methods

Density Functional Methods. All quantum chemical calculations were carried out using the ADF[35] program using dispersion-corrected density functional theory (Grimme's DFT-D3 correction with Becke-Johnson damping)[36] at the BLYP-D3(BJ)/TZ2P[37] level of theory. Vibrational analysis confirmed energy minima (no imaginary frequencies) and transition states (a single imaginary frequency).[38] The all electron TZ2P basis set is of triple-ζ quality, augmented by two sets of polarization functions (3*d* and 4*f* on C, N, O; 2*p* and 3*d* on H) and consists of a large uncontracted set of Slater-type orbitals used to construct the molecular orbitals (MOs). The accuracy parameter of both the Becke grid integration and ZLMfit were set to VERYGOOD.[39] Solvation effects are approximated using the COSMO model, which defines a cavity surrounding the molecule and then applies a dielectric continuum.[40] Optimized structures were illustrated using CYLview.[41]

Thermochemistry. For the thermochemistry calculations of the stepwise coordination reactions we used a standard approach. Geometries were optimized and the vibrational frequencies were obtained through numerical differentiation of the analytical gradient.[35a] Enthalpies at 298.15 K and 1 atm ($\Delta H°$) were calculated from the electronic bond energies and vibrational frequencies by using a standard thermochemistry relation for an ideal gas [Eq. (1)].[42]

$$\Delta H° = \Delta E_{trans,\,298} + \Delta E_{rot,\,298} + \Delta E_{vib,\,0} + \Delta(\Delta E_{vib,\,298}) + \Delta(pV) \quad (1)$$

$\Delta E_{trans,\,298}$, $\Delta E_{rot,\,298}$, and $\Delta E_{vib,\,0}$ are the differences between the reactants in the translational, rotational,

and zero-point vibrational energy, respectively, whereas $\Delta E_{vib,\,298}$ takes the vibrational energy change upon going from 0 to 298.15K into account. The vibrational energy corrections and the entropic term $T\Delta S°$ are based on frequency calculations. Thermal corrections for the electronic term are neglected and $\Delta(pV)\approx\Delta(nRT)$ was used. The change of the Gibbs free energy (ΔG) in both the gas and condensed phase was then calculated for 298.15 K and 1 atm ($\Delta G°$) [Eq. (2)].

$$\Delta G° = \Delta H – T\Delta S° \quad (2)$$

NMR Calculations. The NMR spin-spin coupling constants were obtained by finite-field (Fermi-contact) double perturbation theory at the ZORA-B3LYP/QZ4P[43] level using the CPL program[44] as implemented in ADF. B3LYP has been shown to accurately calculate coupling constants in a previous study.[45] The QZ4P basis is of quadruple-ζ quality, augmented by four sets of polarization functions (two 3*d* and two 4*f* sets on C, N, O; two 2*p* and two 3*d* sets on H). Solvation effects in chloroform were accounted for using COSMO.

Supplementary Information

Supporting information for this article is given via a link at the end of the document.

Acknowledgements

M. W. P. and K. M. R. thank Katie McGeough, Chengsheng Chen, and Anniefer Magpusao for the initial synthesis of compound **6**. Anniefer Magpusao, Brandon Q. Mercado at the Yale CBIC are acknowledged for X-ray crystallography of compound **7**. The NSF partially supported this work through a grant to MWP (CHE-0957626).

F. M. B. and T. A. H. thank the Netherlands Organization for Scientific Research (NWO) for financial support through the Planetary and Exo-Planetary Science program (PEPSci) and the Dutch Astrochemistry Network (DAN).

References

[1] a) A. K. Yudin, *Chem. Sci.* **2015**, *6*, 30–49; b) F. Giordanetto, J. Kihlberg, *J. Med. Chem.* **2014**, *57*, 278–295; c) J. Mallinson, I. Collins, *Future Med. Chem.* **2012**, *4*, 1409–1438; d) E. M. Driggers, S. P. Hale, J. Lee and N. K. Terrett, *Nat. Rev. Drug Discovery*, **2008**, *7*, 608–624.

[2] E. A. Villar, D. Beglov, S. Chennamadhavuni, J. A. Porco Jr, D. Kozakov, S. Vajda, A. Whitty, *Nat. Chem. Biol.* **2014**, *10*, 723–731.

[3] Y.-K. Kim, M. A. Arai, T. Arai, J. O. Lamenzo, E. F. Dean III, N. Peterson, P. A. Clemons, S. L. Schreiber, *J. Am. Chem. Soc.* **2004**, *126*, 14740–14745.

[4] S. U. Aleem, G. Georghio, R. E. Kleiner, K. E. Guja, B. P. Craddock, A. Lyczek, A. I. Chan, M. Garcia-Diaz, W. T. Miller, D. R. Liu, M. A. Seeliger, *Cell Chem. Biol.* **2016**, *23*, 1103-1113.

[5] E. Marsault, M. L. Peterson, *J. Med. Chem.* **2011**, *54*, 1961–2004.

[6] E. M. Larsen, M. R. Wilson, R. E. Taylor, *Nat. Prod. Rep.* **2015**, *32*, 1183–1206.

[7] R. W. Hoffmann *Angew. Chem. Int. Ed. Engl.* **1992**, *31*, 1124–1134.

[8] Y. Liu, A. Singharoy, C. G. Mayne, A. Sengupta, K. Ragavachari, K. Schulten, A. H. Flood, *J. Am. Chem. Soc.* **2016**, *138*, 4843–4851.

[9] a) S. L. Schreiber, *Science* **2000**, *287*, 1964–1969; b) M. D. Burke, E. M. Berger, S. L. Schreiber, *Science* **2003**, *302*, 613–618; c) J. K. Sello, P. R. Andreana, D. Lee, S. L. Schreiber, *Org. Lett.* **2003**, *5*, 4125–4127; d) J. Blankenstein, J. Zhu, *Eur. J. Org. Chem.* **2005**, 1949–1964.

[10] D. Lee, J. K. Sello, S. L. Schreiber, *J. Am. Chem. Soc.* **1999**, *121*, 10648–10649.

[11] a) J. Ma, M. W. Peczuh, *J. Org. Chem.* **2013**, *78*, 7414–7422; b) A. N. Magpusao, K. Rutledge, B. Q. Mercado, M. W. Peczuh, *Org. Biomol. Chem.* **2015**, *13*, 5086–5089; c) A. N. Magpusao, K. Rutledge, T. A. Hamlin, J. M. Lawrence, B. Q. Mercado, N. E. Leadbeater, M. W. Peczuh, *Chem. Eur. J.* **2016**, *22*, 6001–6011.

[12] W. S. Fyvie, M. W. Peczuh, *J. Org. Chem.* **2008**, *73*, 3626–3629.

[13] W. S. Fyvie, M. W. Peczuh, *Chem. Commun.* **2008**, 4028–4030.

[14] J. Ma, R. Vannam, D. W. Terwilliger, M. W. Peczuh, *Tetrahedron Lett.* **2014**, *55*, 4255–4259.

[15] a) D. Si, M. W. Peczuh, *Carbohydr. Res.* **2016**, *434*, 113–120; b) D. Si, M. W. Peczuh, *Org. Biomol. Chem.* **2015**, *13*, 6463–6467.

[16] C. Trigili, I. Barasoain, P. A Sánchez-Murcia, K. Bargsten, M. Redondo-Horcajo, A. Nogales, N. M. Gardner, A. Meyer, G. J. Naylor, E. Gómez-Rubio, F. Gago, M. O. Steinmetz, I. Paterson, A. E. Prota, J. F. Díaz, *ACS Omega* **2016**, *1*, 1192–1204.

[17] H. Fuwa, K. Mizunuma, M. Sasaki, T. Suzuki, H. Kubo, *Org. Biomol. Chem.* **2013**. *11*, 3411–3574.

[18] a) A. Gabba, S. Robakiewicz, B. Taciak, K. Ulewicz, G. Broggini, G. Rastelli, M. Krol, P. V. Murphy, D. Passarella, *Eur. J. Org. Chem.* **2017**, 60–69; b) D. L. Re, Y. Zhou, J. Mucha, L. F. Jones, L. Leahy, C. Santocanale, M. Krol, P. V. Murphy, *Chem. Eur. J.* **2015**, *21*, 18109–18121; c) W. Tu, P. E. Floreancig, Angew. Chem. Int. Ed. 2009, 48, 4567–4571; d) T. E. Rose, K. V. Lawson, P. G. Harran, *Chem. Sci.* **2015**, *6*, 2219–2223.

[19] a) Q. H. Chen, P. N. P. Rao, E. E. Knaus, *Bioorganic Med. Chem.* **2005**, *13*, 4694–4703; b) M.; Pour, M. Spulak, V. Buchata, P. Kubanova, M. Voprsalova, V. Wsol, H. Fakova, P. Koudelka, H. Pourova, R. Schiller, *J. Med. Chem.* **2001**, *44*, 2701–2706.

[20] E. A. Couladouros, I. C. Soufli, V. I. Moutsos, R. K. Chadha, *Chem. Eur. J.* **1998**, *4*, 33–43.

[21] V. Mojr, E. Svobodová, K. Straková, T. Neveselý, J. Chudoba, H. Dvořáková, R. Cibulka, *Chem. Commun.* **2015**, *51*, 12036–12039.

[22] D. A. Devalankar, P. U. Karabal, A. Sudalai, *Org. Biomol. Chem.* **2013**, *11*, 1280–1285.

[23] Details on the synthesis of acids **2** and **3** can be found in the Supplementary Information.

[24] O. Atasoylu, G. Furst, C. Risatti, A. B. Smith, *Org. Lett.* **2010**, *12*, 1788–1791.

[25] E. M. Larsen, M. R Wilson, J. Zajicek, R. E. Taylor, *Org. Lett.* **2013**, *15*, 5246–5249.

[26] Tables for the dihedrals and coupling constants can be found in the Supplementary Information.

[27] https://www.chem.wisc.edu/areas/reich/nmr/05-hmr-05-3j.htm

[28] N. L. Allinger, M. T. Tribble *Tetrahedron Lett.* **1971**, *12*, 3259–3262.

[29] W. F. Bailey, K. M. Lambert, K. B. Wiberg, B. Q. Mercado *J. Org. Chem.* **2015**, *80*, 4108–4115.

[30] a) W. C. Still, *J. Am. Chem. Soc.* **1979**, *101*, 2493–2495; b) W. C. Still, I. Galynker, *Tetrahedron* **1981**, *37*, 3981–3996; c) C. Han, S. Rangarajan, A. Voukides, A. B. Beeler, R. Johnson, J. A. Porco, *Org. Lett.* **2009**, *11*, 413–416; d) W. C. Still, A. G. Romero, *J. Am. Chem. Soc.* **1986**, *108*, 2105–2106; e) S. Arns, M. Lebrun, C. M. Grise, I. Denissova, L. J. Barriault, *J. Org. Chem.* **2007**, *72*, 9314–9322.

[31] a) R. W. Murray, M. Singh, *Org. Synth.***1997**, *74*, 91–100; b) M. Gilbert, M. Ferrer, F. Sanchez-Baeza, A. Messeguer, *Tetrahedron* **1997**, *53*, 8643–8650.

[32] C. Jenson, J. Liu, K. N. Houk, W. L Jorgensen, *J. Am. Chem. Soc.* **1997**, *119*, 12982–12983.

[33] a) Bickelhaupt, F. M.; Houk, K. N. *Angew. Chem. Int. Ed.* **2017**, *in press*; b) L. P. Wolters and F. M. Bickelhaupt, *WIRES Comput. Mol. Sci*., **2015**, *5*, 324–343; c) I. Fernández and F. M. Bickelhaupt, *Chem. Soc. Rev.*, **2014**, *43*, 4953–4967; d) W.-J van Zeist and F. M. Bickelhaupt, *Org. Biomol. Chem.*, **2010**, *8*, 3118–3127.

[34] a) D. H. Ess and K. N. Houk, *J. Am. Chem. Soc.*, **2008**, *130*, 10187–10198; b) D. H. Ess, G. O. Jones and K. N. Houk, *Org. Lett*, **2008**, *10*, 1633–1636; c) D. H. Ess and K. N. Houk, *J. Am. Chem. Soc.*, **2007**, *129*, 10646–10647.

[35] a) G. te Velde; F. M. Bickelhaupt, E. J. Baerends, C. Fonseca Guerra, S. J. A. van Gisbergen, J. G. Snijders, T. Ziegler, *J. Comput. Chem.* **2001**, *22*, 931−967. b) Fonseca Guerra, C.; Snijder, J. G.; te

Velde, G.; Baerends, E. J. *Theor. Chem. Acc.* **1998**, *99*, 291. c) ADF2016, SCM, Theoretical Chemistry, Vrije Universiteit, Amsterdam, The Netherlands, http://www.scm.com.

[36] a) S. Grimme, J. Antony, S. Ehrlich and S. Krieg, *J. Chem. Phys.*, **2010**, *132,* 154104–154104; b) A. D. Becke and E. R. Johnson, *J. Chem. Phys.*, **2005**, *123*, 154101.

[37] a) A. D. Becke, *Phys. Rev. A*, **1988**, *38*, 3098–3100; b) C. Lee, W. Yang and R. G. Parr, *Phys. Rev. B*, **1988**, *37*, 785–789; c) E. V. Lenthe and E. J. Baerends, *J. Comp. Chem.*, **2003**, *24*, 1142–1156.

[38] L. Y. Fan, L. Versluis, T. Ziegler, E. J. Baerends, W. Ravenek, *Int. J. Quantum Chem.* **1988**, *34*, 173−181.

[39] a) A. D. Becke, *J. Chem. Phys.* **1988**, *88*, 2547; (b) M. Franchini, P. H. T. Philipsen, L. Visscher, *J. Comput. Chem.* **2013**, *34*, 1818–1827.

[40] a) A. Klamt and G. Schüürmann, *J. Chem. Soc. Perkin Trans. 2*, **1993**, *2*, 799–805; b) A. Klamt, *J. Phys. Chem.*, **1995**, *99*, 2224–2235; c) A. Klamt and V. Jones, *J. Chem. Phys.*, 1996, **105**, 9972–9981.

[41] C. Y. Legault, CYLview, 1.0.562 BETA; Université de Sherbrooke: Sherbrooke, Quebec, Canada, 2009. http://www.cylview.org

[42] F. Jensen, Introduction to Computational Chemistry, 2nd ed., Wiley, Chichester, 2007.

[43] a) E. van Lenthe, E. J. Baerends, J. G. Snijders, *J. Chem. Phys.* **1993**, *99*, 4597; b) E. van Lenthe, E. J. Baerends, J. G. Snijders, *J. Chem. Phys.* **1994**, *101*, 9783; c) E. van Lenthe, A. Ehlers, E. J. Baerends, *J. Chem. Phys.* **1999**, *110*, 8943.

[44] a) J. Autschbach, T. Ziegler, *J. Phys. Chem.*, **2000**, *113*, 936–947; b) J. Autschbach, T. Ziegler, *J. Phys. Chem.*, **2000**, *113*, 9410–9418.

[45] a) O. E. Taurian, D. G. De Kowalewski, J. E. Pérez, R. H. Contreras, *J. Mol. Struct.* **2005**, *754*, 1–9; b) M. Tafazzoli, M. *Carbohydr. Res.* **2007**, *342*, 2086–2096.